RSC Advances

PAPER

View Article Online
View Journal | View Issue

Cite this: *RSC Adv.*, 2018, **8**, 6356

Molecular solar thermal systems – control of light harvesting and energy storage by protonation/deprotonation†

Martin Drøhse Kilde, ‡ Paloma Garcia Arroyo, ‡ Anders S. Gertsen, ‡§ Kurt V. Mikkelsen and Mogens Brøndsted Nielsen *

Received 30th December 2017
Accepted 1st February 2018

DOI: 10.1039/c7ra13762a

rsc.li/rsc-advances

Molecular solar thermal (MOST) systems that undergo photoisomerizations to long-lived, high-energy forms present one approach of addressing the challenge of solar energy storage. For this approach to mature, photochromic molecules which can absorb at the right wavelengths and which can store a sufficient amount of energy in a controlled time period have to be developed. Here we show in a combined experimental and theoretical study that incorporation of a pyridyl substituent onto the dihydroazulene/vinylheptafulvene photo-/thermoswitch results in molecules whose optical properties, energy-releasing back-reactions and energy densities can be controlled by protonation/deprotonation. The work thus presents a proof-of-concept for using acid/base to control the properties of MOST systems.

Introduction

Efficient exploitation of solar energy is a major challenge for meeting the increasing energy demands of the world. Development of organic molecules for photovoltaics has for this reason attracted considerable focus. Light-harvesting, energy storage, and ultimately heat release by photochromic molecules, in brief molecular solar thermal (MOST) systems, has been an alternative niche area, which in recent years, however, has attracted attention.[1] MOST systems correspond to closed-energy cycles with no release of CO_2 or other oxidation products. Photochromic molecules are interchangeable upon stimuli with light in at least one direction. The practical criteria for MOST systems are in particular sufficiently large energy densities (an upper limit is probably 1 MJ kg^{-1} corresponding to that of the norbornadiene/quadricyclane couple[2]) and the ability to release the stored energy in a controlled manner when needed.

The yellow dihydroazulene (DHA; 2-phenyl-1,8a-dihydroazulene-1,1-dicarbonitrile)[3] is a one-way photoswitch with a high quantum yield[4] of photoisomerization. Upon irradiation at its lowest-energy absorption maximum (*ca.* 350 nm), DHA converts to its higher energy isomer, the red vinylheptafulvene (VHF; Scheme 1).[3] Upon ring-opening, the VHF is formed as its s-*cis* conformer, which rapidly changes to the more stable s-*trans* conformer.[5] As the back-reaction has to proceed through the s-*cis* VHF, its rate depends on both the position of the s-*trans*/s-*cis* pre-equilibrium and the activation energy of ring closure. Fine-tuning of the rate of the thermal back-reaction is possible with changes in solvent polarity[6] and electronic character of substituent groups.[7] The DHA/VHF system has many different positions to functionalize and with synthetic protocols in hand, the study of structural modifications at various positions has been possible providing both ultrafast ring closures and very stable VHFs.[8] For example, bridging the DHA and the phenyl substituent by a $-CH_2CH_2-$ linker as in the "dihydronaphthalene–DHA" (DHN–DHA) sketched in Scheme 1

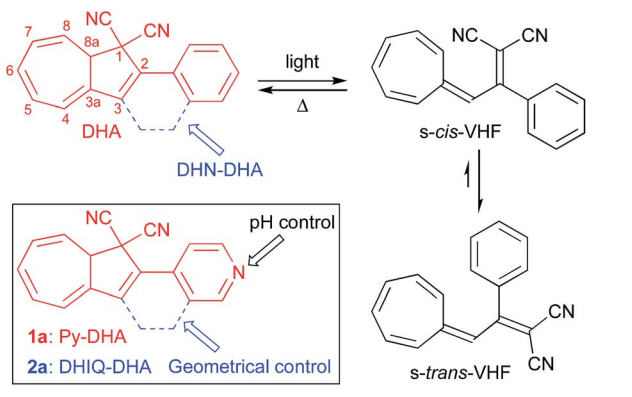

Scheme 1 Photo/thermal switching of the dihydroazulene (DHA)/vinylheptafulvene (VHF) system. By incorporating a CH_2CH_2 bridge (indicated in blue color), a locked dihydronaphthalene–DHA (DHN–DHA) is obtained. Inset: pH controllable DHAs: pyridyl-DHA (Py-DHA, **1a**) and the locked dihydroisoquinoline-DHA (DHIQ-DHA, **2a**).

Department of Chemistry, University of Copenhagen, Universitetsparken 5, 2100 Copenhagen, Denmark. E-mail: mbn@chem.ku.dk

† Electronic supplementary information (ESI) available: Synthesis protocols, NMR spectra, switching studies and computational data. See DOI: 10.1039/c7ra13762a

‡ These authors contributed equally to the article.

§ Present address: Department of Energy Conversion and Storage, Technical University of Denmark, Frederiksborgvej 399, DK-4000 Roskilde, Denmark.

results in almost instantaneous ring closure of the resulting VHF as it is locked in its reactive s-*cis* conformation.[8a] The parent DHA/VHF system only provides an energy density[9] of 0.11 MJ kg^{-1} and a VHF half-life of 218 min (MeCN, 25 °C).[6] Yet, even minor structural changes can greatly enhance the energy storage capacity.[8b,10]

Hecht and co-workers[11] have recently demonstrated how acid can be used to trigger release of stored light energy in the thermal cycloreversion of a diarylethene.[12] Previous work on the DHA/VHF system[13] has employed protonation/deprotonation of an anilino substituent group to control switching properties, and we became interested to further explore the concept of acid/base control by incorporating a basic pyridine group. Here we demonstrate the synthesis, optical and switching properties and theoretical investigations of proof-of-concept systems, "pyridyl-DHA" **1a** (Py-DHA) and "dihydroisoquinoline-DHA" **2a** (DHIQ-DHA) (Scheme 1). The pyridine ring provides *via* the basic nitrogen a handle for controlling the VHF-to-DHA back-reaction by protonation as well as for tuning the absorption maxima and energy storage capacities. Our investigations were driven by an initial computational screening of potential interesting systems and based on the initial computational screening, relevant systems were selected for experimental work and more detailed calculations.

Results and discussion

Synthesis

Synthesis of **1a** started with a Knoevenagel condensation between 4-acetylpyridine and malononitrile in HMDS/AcOH which furnished the adduct **4** (Scheme 2). This compound was thermally unstable, and prolonged heating as well as purification by column chromatography resulted in degradation products. Therefore, **4** was just used in the next step after aqueous work-up (with only minor impurities remaining). Addition of tropylium tetrafluoroborate and Et_3N in MeCN at room temperature (rt) gave the VHF-precursor **5** in good yield, which easily could be obtained on large scale after dry-column vacuum chromatographic work-up. Oxidation of VHF-precursors has previously shown to be a tedious step,[8] which was also the case in the present case. In a first attempt, tritylium tetrafluoroborate was used as a hydride abstractor in refluxing 1,2-dichloroethane. However, this attempt was fruitless, giving no desired product formation even after prolonged refluxing. Instead we turned to nitrosonium tetrafluoroborate ($NOBF_4$) in MeCN at −40 °C followed by the addition of dilute pyridine in CH_2Cl_2; this in turn yielded the distinct red VHF (as observed on TLC), which after heating to reflux thermally cyclized to Py-DHA **1a**. The pyridyl nitrogen serves as a convenient site for further chemistry. Thus, methylation of **1a** was achieved by treatment with MeI in MeCN to yield the salt **6a** in quantitative yield.

To obtain the locked dihydroisoquinoline-DHA **2a**, the commercially available 5,6,7,8-tetrahydroisoquinoline **7** was used as starting material in initial steps following literature protocols[14] (Scheme 3). Oxidation with H_2O_2 in AcOH gave the N-oxide **8**, which underwent Polonovski rearrangement in refluxing acetic anhydride to provide the acetoxy product **9**. Hydrolysis of this compound in acidic media (10% aq. HCl) followed by oxidation led finally to the desired ketone **11** in an overall yield of 22% starting from **5**.[14] Then, Knoevenagel condensation of **11** with malononitrile and NH_4OAc/AcOH buffer in toluene gave **12**, which was turned into the corresponding VHF-precursor **13** by treatment with tropylium tetrafluoroborate and Et_3N in MeCN at rt, with both reactions being high-yielding (87 and 80%, respectively). The obtained VHF-precursor **13** turned out to be even more challenging to oxidize than **4**. First, we tried using the same conditions as for **4**; **13** was treated with $NOBF_4$ in MeCN at −40 °C followed by the addition of dilute pyridine in CH_2Cl_2, but no desired product could be detected or isolated. Instead, treating the tropylium cationic intermediate with the stronger base DBU gave DHIQ-DHN **2a** in 6% yield, after ring closure of the intermediate VHF isomer **2b**. Unfortunately, this procedure was not

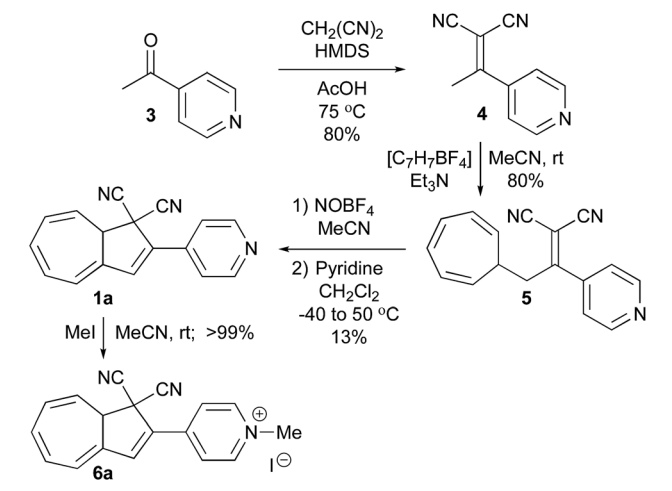

Scheme 2 Synthesis of Py-DHA **1a** and further methylation at the pyridyl nitrogen to yield the salt **6a**. HMDS = hexamethyldisilazane.

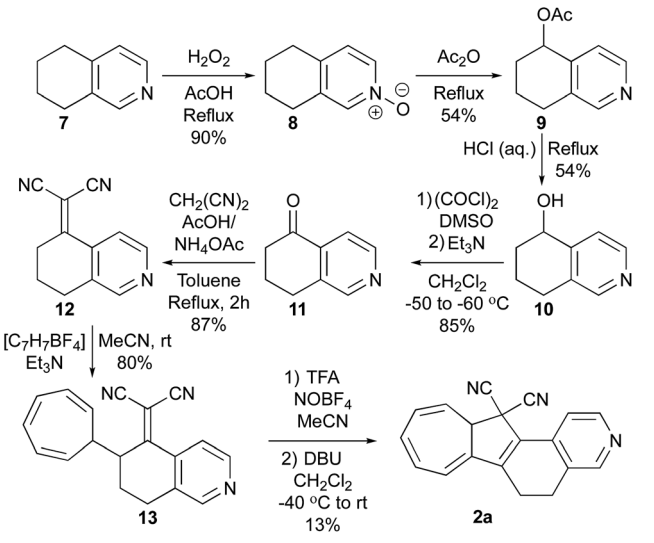

Scheme 3 Synthesis of DHIQ-DHN **2a**. DBU = 1,8-diazabicyclo[5.4.0]undec-7-ene.

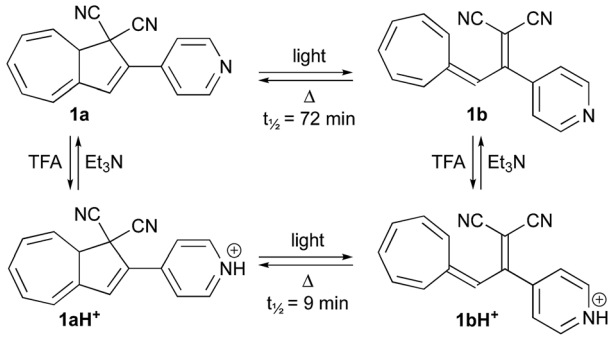

Scheme 4 Multimode switch based on acid/base and light/heat stimuli. TFA = trifluoroacetic acid.

reproducible, and we could only isolate **2a** on one occasion. On the other hand, if the VHF-precursor **13** was first protonated by trifluoroacetic acid (TFA) and then treated with the hydride abstractor ($NOBF_4$) and DBU, we could isolate **2a** in an improved yield of 13%. The overall yield of **2a** from **7** is 2% while that of **1a** is 8% from the starting material **3**.

Multimode switching studies

With the novel photoswitches Py-DHA **1a** and DHIQ-DHA **2a** in hand, their photophysical and photochemical properties were studied, including the influence of protonation of the basic nitrogens (Scheme 4). UV/Vis absorption spectroscopy studies of Py-DHA **1a** were conducted in MeCN at 25 °C and the results compared in Table 1 to its respective carbon analogue (DHA,[6] shown in Scheme 1). Py-DHA **1a** could easily be converted to VHF **1b** upon light irradiation (365 nm), seen by a distinctive redshifted absorption band appearing, going from 1a (λ_{max} = 359 nm) to **1b** (λ_{max} = 480 nm) (Fig. 1, top). Then, **1b** thermally relaxed to **1a** (Fig. 1, bottom). By plotting the decay of the VHF absorbance at 480 nm against time (first-order kinetics), an exponential fit provided the rate constant. The pyridyl-substituent at **1b** induced an increased rate of back-reaction compared to the carbon analogue (VHF); half-lives of $t_{1/2}$ = 72 min and 218 min, respectively, as expected when incorporating an electron-withdrawing substituent.[7] Next, we studied

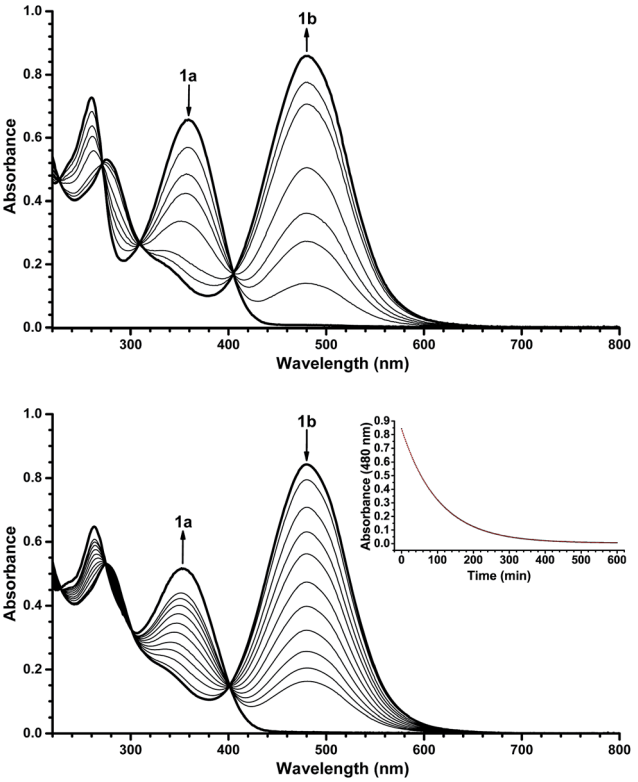

Fig. 1 UV/Vis absorption spectra recorded at 25 °C in MeCN. Top: Acquired during the ring-opening of Py-DHA **1a** to **1b**. Bottom: Acquired during the ring closure of **1b** to **1a**. Inset: Decay of VHF absorbance (at 480 nm) against time (min) (first-order kinetics).

the influence of protonation of Py-DHA **1a** with ^{1}H-NMR and UV/Vis spectroscopies. Firstly, the gradual protonation of Py-DHA **1a** was followed by ^{1}H NMR spectroscopy using trifluoroacetic acid (TFA) in $CDCl_3$ at 300 MHz (Fig. 2). Upon protonation, all proton resonances moved downfield, and not only those assigned to the pyridyl ring. Chemical shifts of **1a** and **1aH$^+$** are listed in Table 2. Secondly, gradual protonation with TFA in MeCN was easily followed with UV/Vis absorption spectroscopy in which isosbestic points were observed going from Py-DHA **1a** (359) to more redshifted **1aH$^+$** (λ_{max} = 406 nm) (Fig. 3). Addition of Et_3N to **1aH$^+$** resulted in deprotonation and

Table 1 Summary of absorption and kinetics data (VHF-to-DHA conversion)

	Solvent	DHA λ_{max} [nm]	VHF λ_{max} [nm]	Temp. [°C]	k [min^{-1}] VHF → DHA	$t_{1/2}$ [min]
DHA/VHF[a]	MeCN	353	470	25	0.0032	218
1a/**1b**	MeCN	359	480	25	0.0097	72
1a/**1b**[b]	MeCN	359	480	25	0.0101	69
1aH$^+$/**1bH$^+$**[c]	MeCN	406	483	25	0.0770	9
6a	MeCN	407				
DHN–DHA/DHN–VHF[d]	EtOH	365	476	−50	0.313	2.2
2a/**2b**	EtOH	364	440	−50	0.0079	88
2aH$^+$/**2bH$^+$**	EtOH	380	—	Varying	—	—

[a] Ref. 6. [b] Obtained by addition of 20 equiv. TFA and 20 equiv. Et_3N. [c] Kinetics data obtained after addition of 20 equiv. TFA (absorption maxima: DHA 402 nm at 20 equiv. TFA and 406 nm at 200 equiv. TFA; VHF 483 nm at 20 equiv. TFA). [d] Ref. 8*a*.

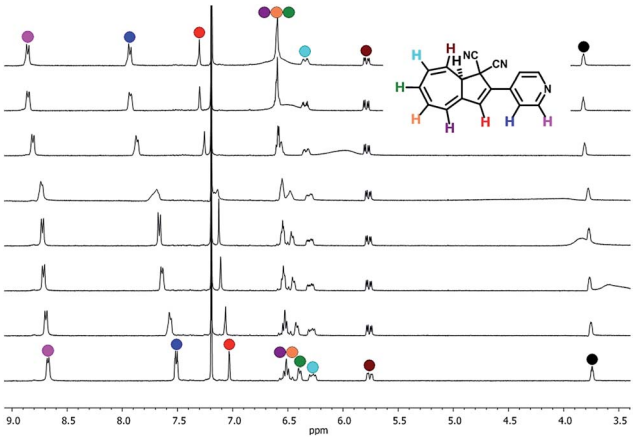

Fig. 2 Stacked ^{1}H-NMR spectra recorded upon protonation of **1a** (bottom) to **1aH$^+$** (top) with TFA in $CDCl_3$ (300 MHz); each spectrum corresponds to subsequent addition of 0.2 equiv. of TFA.

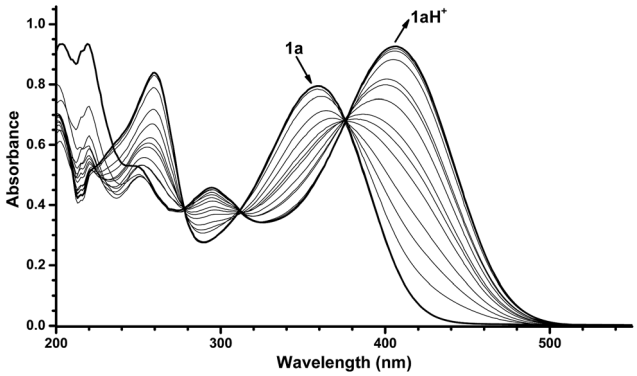

Fig. 3 UV/Vis absorption spectra resulting from protonation of Py-DHA **1a** (7.0×10^{-5} mol L^{-1}) with TFA in MeCN. The spectra presented are in the range of 0 equiv. TFA to 200 equiv. TFA. For full details of protonation, see ESI.†

the initial **1a** was obtained as determined by UV/Vis spectroscopy (Fig. S31, ESI†). The protonated species **1aH$^+$** also showed photochromism, and the thermal back-reaction of **1bH$^+$** was 8-fold faster than that of **1b** ($t_{1/2}$ = 9 min and 72 min, respectively). We also investigated whether the pyridyl could act as a handle for triggering the heat release when needed. Thus, Py-DHA **1a** was turned into its corresponding VHF **1b**, which was voluntarily allowed to return to **1a**. After at least one half-life, TFA was added, resulting in a dramatic enhancement of the thermal back-reaction. After one additional half-life, Et_3N was added, and the rate of back-reaction decreased again, albeit not to exactly the same rate as before the acid–base treatment (Fig. 4). It should be emphasized that some degradation also seems to occur in MeCN during one opening-closure cycle despite the isosbestic points.

The *N*-methyl pyridinium salt **6a** exhibits a characteristic absorption maximum at 407 nm in MeCN, close to that observed for the protonated form of **1a** (λ_{max} 406 nm). While this band slowly decreased upon irradiation (365 nm) and spectral changes occurred with isosbestic points, no characteristic VHF absorption band was observed. Rather than photoisomerization, prolonged irradiation thus seems instead to lead to a chemical conversion of **6a**, possibly into the fully conjugated azulene by elimination of HCN (supported by ^{1}H-NMR spectroscopy by disappearance of the characteristic signal for the **8a** proton), but this was not investigated in further detail.

Table 2 ^{1}H-NMR chemical shifts of **1a** and **1aH$^+$** in $CDCl_3$

H	**1a** δ [ppm]	**1aH$^+$** δ [ppm]	$\Delta\delta$
8a	3.81	3.89	0.08
8	5.83	5.85	0.02
7	6.34	6.40	0.06
6	6.55	6.66	0.11
5	6.61	6.68	0.07
4	6.46	6.64	0.18
3	7.09	7.37	0.28
β-Py	8.74	8.93	0.19
α-Py	7.57	8.00	0.03

The isoquinoline moiety in the DHIQ-DHA **2a**/**2b** system forces the VHF to be in the s-*cis* conformation. Hence, the thermal back-reaction is very fast, and we had to retard it by cooling when acquiring the absorption spectrum of the VHF **2b** in EtOH. Thus, DHIQ-DHA **2a** was cooled to −50 °C and upon light irradiation (365 nm), it turned into the VHF **2b**, seen by a distinctive redshifted absorption band appearing, going from **2a** (λ_{max} = 364 nm) to **2b** (λ_{max} = 440 nm) (Fig. 5, top). Then, **2b** thermally relaxed to **2a** (Fig. 5, bottom). By plotting the decay of VHF, **2b**, absorbance at 440 nm against time (first-order kinetics) an exponential fit provided the half-life to be 88 min at −50 °C in EtOH. Interestingly, when comparing the half-life of **2b** to that of the related DHN–DHA system, the half-life of **2b** is 40-fold longer. Currently, we cannot rationalize this result, since the electron-withdrawing pyridyl is expected to enhance the ring closure (as seen for **1b**). Density functional theory calculations also suggest that this intuition is correct, yielding

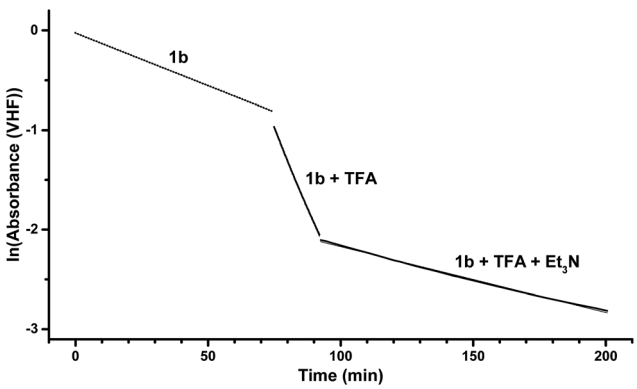

Fig. 4 Natural logarithm (ln) of the VHF absorbance (at a wavelength of 480 nm for **1b** and **1b** + **TFA** + **Et$_3$N** mixture and at 483 nm for **1b** + **TFA** mixture) against time. The thermal heat release is activated by addition of TFA (steep slope) and the heat release is retarded again upon addition of Et_3N.

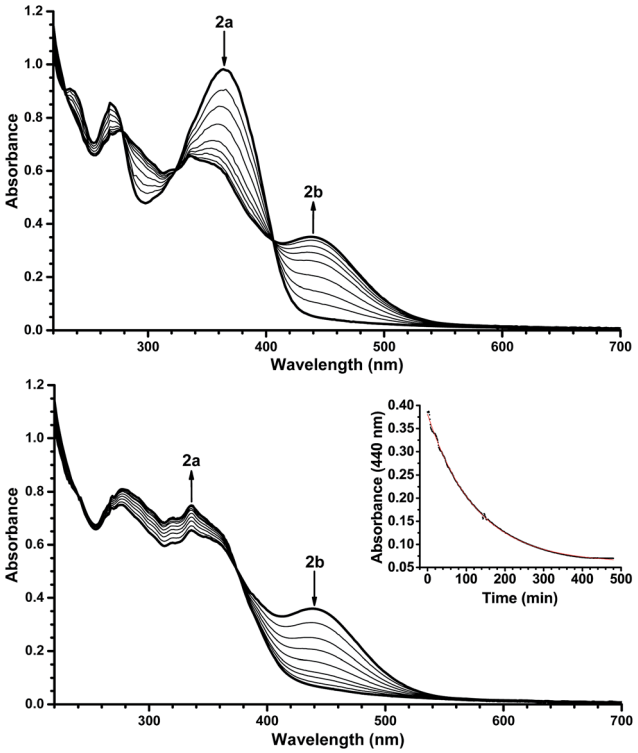

Fig. 5 UV/Vis absorption spectra recorded at −50 °C in EtOH. Top: Acquired during the ring-opening of DHIQ-DHA **2a** to **2b**. Bottom: Acquired during the ring closure of **2b** to **2a**. Inset: Decay of VHF absorbance (440 nm) against time (min) (first-order kinetics).

thermal back-reaction barriers for the **2b** ring closure that are consistently 5 kJ mol^{-1} lower than those of the DHN–VHF (*vide infra*).

Protonation of **2a** with TFA in abs. EtOH at 25 °C was easily followed with UV/Vis absorption spectroscopy, revealing a redshift in the characteristic DHA absorption (Fig. 6). Irradiation (365 nm) of **2aH$^+$** (at various temperatures in the interval from −70 to 25 °C) gave no changes in the absorption spectrum. Instead, the cuvette took upon a blue fluorescent color (Fig. 7,

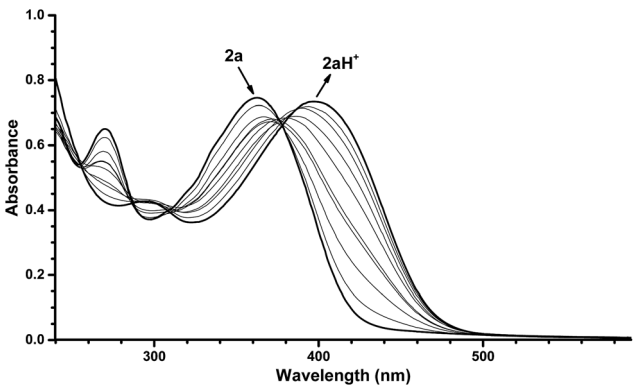

Fig. 6 UV/Vis absorption spectra resulting from protonation of DHIQ-DHA **2a** (6.6×10^{-5} mol L^{-1}) with TFA in EtOH. The spectra presented are in the range of 0 equiv. TFA to 400 equiv. TFA. For full details of protonation, see ESI.†

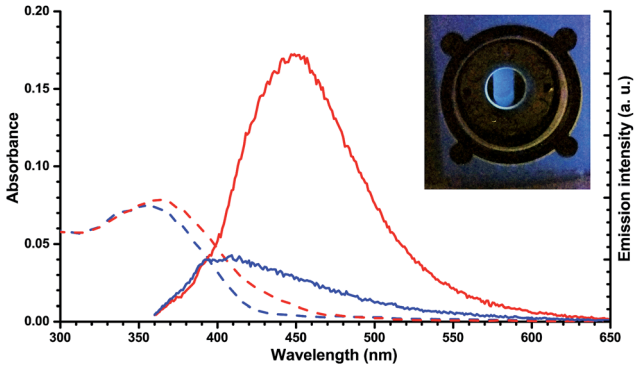

Fig. 7 UV/Vis absorption (broken line) and emission (full line) spectrum of **2a** (blue) and **2aH$^+$** (with 20 equiv. TFA; red) in abs. EtOH at 25 °C. Inset: Photo of the cuvette of **2aH$^+$** upon light irradiation (365 nm) inside the cryostat at −50 °C.

inset). The emission spectra of **2aH$^+$** and the non-protonated **2a** are shown in Fig. 7. We cannot exclude an ultrafast back-reaction of **2bH$^+$**, if formed, but the apparent lack of photoisomerization of **2aH$^+$** may partly be accounted for by its stronger fluorescence than that of the unprotonated **2a**. No apparent fluorescence is visible by the naked eye for **1a** and **1aH$^+$** at room temperature.

Calculations

A computational study was performed in order to shed light on the thermal back-reactions. All calculations were performed in Gaussian 16 (ref. 15) or Gaussian 09 (ref. 16) using density functional theory (DFT). In correspondence with suggestions from previously published benchmark studies,[9] the M06-2X global exchange–correlation functional was employed together with the 6-311++G(d,p) basis-set.[17] The solvent effects in this work are considered both using explicit solvent molecules (hence the inclusion of both diffuse and polarization functions on hydrogens in the basis-set in order to capture specific effects of hydrogen bonding) and the integral equation formalism of the polarizable continuum model (IEFPCM) as well as a combination hereof. In the case of the ethanol solvent (EtOH), hydrogen bonds are believed to be crucial for the observed tendencies, and we chose to include calculations with one ethanol molecule hydrogen-bonded to the pyridine nitrogen (OH···N) or its protonated analogue (O···HN$^+$) in addition to the pure continuum model treatments. We thus considered vacuum and six different media: toluene, CH_2Cl_2, EtOH, and MeCN using IEFPCM, an explicit EtOH molecule in vacuum, and an explicit EtOH molecule combined with EtOH modelled by IEFPCM.

Initially, geometry optimizations of the (8a*R*) stereoisomers of the DHAs and their corresponding VHFs as well as the protonated analogues of all of these were performed and confirmed as minima by harmonic frequency analyses (see ESI† for structures). In correspondence with the literature,[10a] there are two types of VHF → DHA ring closure transition states (TS_P and TS_T) which were located and confirmed as first-order saddle points by harmonic frequency analyses. All systems were then subjected to the solvation schemes described above. The

thermochemical data for these are calculated at a temperature of 203.15 K and a pressure of 1 atm and presented in Table 3. In this table, we report six different thermochemical properties:

(1) The relative transition state stability $\Delta\Delta G_{TS}$ which is calculated as the difference in Gibbs free energy of the TS_P and TS_T transition states, $\Delta\Delta G_{TS} = \Delta G_{TS(P)} - \Delta G_{TS(T)}$.

(2) The relative s-*cis*-VHF/s-*trans*-VHF stability $\Delta\Delta G_{VHF}$ which is calculated as the difference in Gibbs free energy of the s-*cis*-VHF and the s-*trans*-VHF, $\Delta\Delta G_{VHF} = \Delta G_{s\text{-}cis\text{-}VHF} - \Delta G_{s\text{-}trans\text{-}VHF}$ (only relevant for the **1b** and **1bH$^+$** systems) and the corresponding equilibrium constants *K*.

(3) The thermal back-reaction barrier ΔG_{TBR} calculated as the difference in Gibbs free energy of the s-*cis*-VHF and the lowest transition state.

(4) The corrected thermal back-reaction barrier $\Delta G'_{TBR}$ which is corrected for the pre-equilibrium between the s-*cis*-VHF and the s-*trans*-VHF by modifying the rate constant (obtained using the Eyring equation) of the uncorrected back-reaction by a factor $K/(K + 1)$ where *K* is the equilibrium constant of the s-*cis*/s-*trans* conformational change and from this converted back to a corrected Gibbs free energy through the Eyring equation (only relevant for the **1a**/**1b** and **1aH$^+$**/**1bH$^+$** systems).

(5) The energy storage capacity $\Delta H_{storage}$ calculated as the difference in enthalpy between the s-*trans*-VHF and the (8a*R*)-DHA of the **1a**/**1b** and **1aH$^+$**/**1bH$^+$** systems and as the difference in enthalpy between the s-*cis*-VHF and the (8a*R*)-DHA of the **2a**/**2b**, **2aH$^+$**/**2bH$^+$**, and DHN–DHA/DHN–VHF systems.

(6) The energy density calculated as the energy storage capacity divided by the molecular weight of the system.

First, we note that the energy density is significantly increased for the bridged system (**2a**/**2b**) relative to the unbridged one (**1a**/**1b**), independently of the medium. Secondly, for both systems, protonation increases the energy density – in vacuum from 0.142 MJ kg^{-1} (**1a**/**1b**) to 0.231 MJ kg^{-1} (**1aH$^+$**/**1bH$^+$**) and from 0.235 MJ kg^{-1} (**2a**/**2b**) to 0.295 MJ kg^{-1} (**2aH$^+$**/**2bH$^+$**). The energy densities are smaller in polar media, while just adding one hydrogen-bonded ethanol molecule to the pyridine-based systems in vacuum has little effect (hydrogen bonding to the pyridine N or N$^+$H).

In regard to kinetics, we see that, indeed, the locked system **2b** has a lower back-reaction barrier (ΔG_{TBR}) than the unlocked system **1b**, in agreement with experimental findings (*vide supra*). In addition, protonation leads to a very significant lowering of the barrier for both systems, which was also found experimentally for **1b**. For the thermal back-reaction of **2b** we find a lower barrier than for DHN–VHF regardless of the solvent environment. This contrasts, as mentioned and discussed above, the experimental findings, and we have at the moment no explanation for this discrepancy. We note, however, that the

Table 3 Relative transition state stability ($\Delta\Delta G_{TS}$; if negative (positive), TS_P (TS_T) is lower in energy), thermal back-reaction barrier (ΔG_{TBR}), energy storage capacity ($\Delta H_{storage}$) in kJ mol^{-1} and energy density (En. dens.) in MJ kg^{-1}, and equilibrium constant (*K*) for the s-*cis*/s-*trans* VHF conformational change of **1b** for both the neutral and protonated systems in different environments at 203.15 K. An asterisk marks that no TS_T type transition state was located for the given solvation

		Vacuum	PhMe	CH_2Cl_2	EtOH	MeCN	Vacuum + EtOH[a]	EtOH + EtOH[a]
1a/**1b**	$\Delta\Delta G_{TS}$	−8.003	−9.195	−7.937	*	*	−7.821	*
	$\Delta\Delta G_{VHF}$	6.629	7.288	7.610	7.567	7.590	6.569	9.110
	K	0.069	0.053	0.046	0.047	0.047	0.071	0.025
	ΔG_{TBR}	103.9	94.62	87.62	85.68	85.34	104.3	85.74
	$\Delta G'_{TBR}$	110.7	102.0	95.34	93.36	93.05	111.1	94.91
	$\Delta H_{storage}$	36.46	31.52	27.01	25.52	25.24	35.69	25.49
	En. dens.	0.142	0.122	0.105	0.099	0.098	0.139	0.099
1aH$^+$/**1bH$^+$**	$\Delta\Delta G_{TS}$	−9.974	−7.756	*	*	*	−10.95	*
	$\Delta\Delta G_{VHF}$	−6.291	−3.004	3.418	4.797	5.078	−4.135	4.752
	K	12.649	3.359	0.252	0.144	0.129	5.302	0.147
	ΔG_{TBR}	87.83	85.00	78.42	78.19	78.15	89.46	N/A
	$\Delta G'_{TBR}$	88.02	85.64	82.39	83.32	83.53	89.88	N/A
	$\Delta H_{storage}$	59.74	48.82	37.74	34.14	33.45	55.37	29.86
	En. dens.	0.231	0.189	0.146	0.132	0.129	0.214	0.116
2a/**2b**	$\Delta\Delta G_{TS}$	−7.089	−8.966	*	*	*	−9.313	*
	ΔG_{TBR}	93.10	79.62	69.44	66.67	66.14	90.60	65.75
	$\Delta H_{storage}$	66.52	64.39	61.71	60.66	60.43	68.44	61.64
	En. dens.	0.235	0.227	0.218	0.214	0.213	0.241	0.217
2aH$^+$/**2bH$^+$**	$\Delta\Delta G_{TS}$	−13.00	−9.82	*	*	*	−14.07	*
	ΔG_{TBR}	67.84	60.58	56.29	55.52	55.37	70.85	58.84
	$\Delta H_{storage}$	83.62	79.20	72.58	70.27	69.84	79.51	68.65
	En. dens.	0.295	0.279	0.256	0.248	0.246	0.280	0.242
DHN–DHA/DHN–VHF	$\Delta\Delta G_{TS}$	−3.741	−6.782	*	*	*	−0.163	*
	ΔG_{TBR}	97.06	85.03	75.27	72.22	71.64	97.71	72.69
	$\Delta H_{storage}$	64.28	61.08	57.73	56.53	56.29	63.71	56.18
	En. dens.	0.228	0.217	0.205	0.201	0.200	0.226	0.200

[a] One molecule of ethanol was included in the structure, with an OH···N(pyridine) or O···HN$^+$(pyridine) hydrogen bond in the case of the pyridine derivatives.

calculations are in correspondence with the general influence of electron-withdrawing groups that we previously have observed experimentally.[7]

For both **1a** and **2a**, protonation was found experimentally to result in significantly redshifted longest-wavelength absorption maxima. Calculations reveal that the HOMO and LUMO become more localized at each end of the molecule for **1aH**$^+$ and **2aH**$^+$ (Fig. 8), and the transition thus has slightly more charge-transfer character for the protonated species, explaining the observed absorption redshifts.

Calculated UV-Vis absorption spectra of both protonated and non-protonated DHAs **1a** and **2a** provided the same red-shifting influence of protonation as observed in experiment. In Fig. 9, calculated absorption spectra in MeCN for **1a**/**1aH**$^+$ and in EtOH for **2a**/**2aH**$^+$ can be found, both in full qualitative correspondence with experiments (*cf.* Fig. 3 and 6, respectively). The ESI includes spectra in other media. All spectra are determined using linear response TD-DFT at the M06-2X/6-311++G(d,p) level of theory based on the 298.15 K geometries by calculating the 30 lowest energy excited states for each compound. Gaussians with a standard deviation of 0.4 eV were fitted to the oscillator strengths in order to produce the absorption curves. It should be noted that M06-2X has previously been shown to slightly underestimate excitation wavelengths of DHAs,[9] and the observation of this tendency for these compounds too is thus expected.

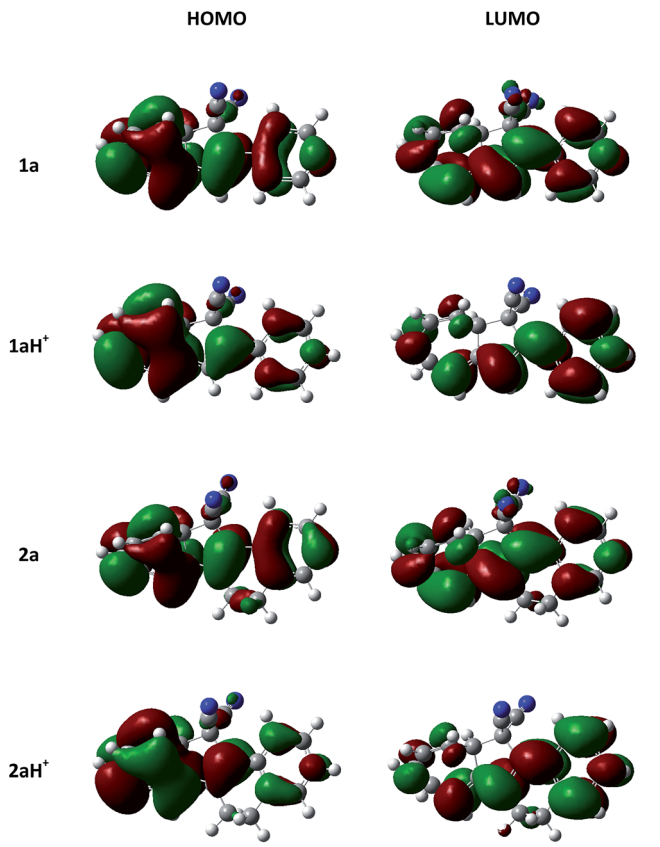

Fig. 8 Computationally determined HOMO and LUMO of **1a**, **1aH**$^+$, **2a**, and **2aH**$^+$ with the M06-2X global exchange–correlation functional and the 6-311++G(d,p) basis-set visualised with an isovalue (contour threshold) of 0.02 au.

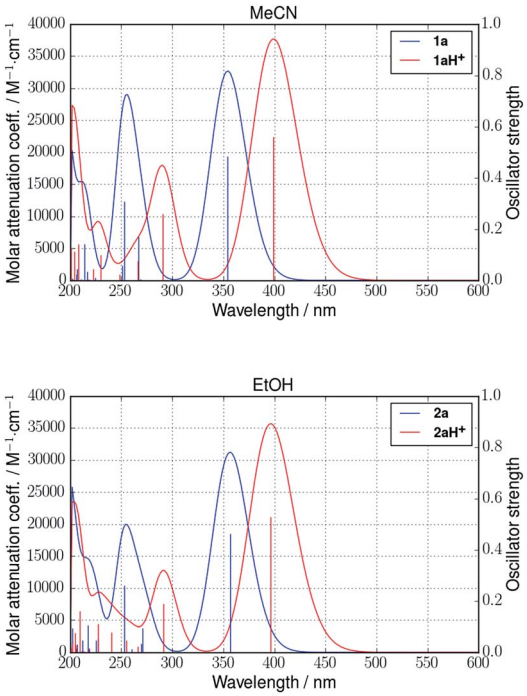

Fig. 9 Calculated absorption spectra of **1a**/**1aH**$^+$ in MeCN (top) and **2a**/**2aH**$^+$ in EtOH (bottom) (linear response TD-DFT, M06-2X/6-311++G(d,p)).

In general, the observed red-shift of DHA absorptions following protonation decreases with increasing solvent polarity for both systems. This is due to the low-energy absorption peaks of the protonated species blue-shifting with increasing solvent polarity, while the low-energy absorption peaks of the non-protonated species remain at almost the same values regardless of solvent. The energies of the low-energy absorption peaks in vacuum and all solvents for VHFs **1b**/**1bH**$^+$ and **2b**/**2bH**$^+$ can be found alongside those of the DHAs **1a**/**1aH**$^+$ and **2a**/**2aH**$^+$ in ESI, Table S2.† These all comply with the above. To summarize, the experimental findings are thus substantiated, and the calculations provide strong indications that protonation of pyridyl-DHAs can serve to red-shift their absorptions toward high solar photon flux spectral ranges without hampering their energy storage capabilities.

Conclusion

Incorporation of a pyridyl substituent onto the dihydroazulene/vinylheptafulvene photo-/thermoswitch was synthetically rather challenging, but we managed to prepare two such derivatives. The pyridine unit acts as a convenient site for controlling properties by protonation/deprotonation. Thus, protonation leads to a significant redshift in the characteristic DHA absorption maximum as the transition gets more charge-transfer character. Protonation can also serve as a method to promote the vinylheptafulvene back-reaction (triggering energy release), and calculations reveal how the energy density is also increased significantly by protonation. Locking the VHF in its s-

cis conformation enhances the energy density, but at the same time, the back-reaction becomes undesirably fast. This may be accounted for by other means; for example, suitable substitution of the core structure can be used to further tune the rate of ring closure.[7] Despite some stability issues (during isolation and during switching cycles), the pyridyl substituent presents in all a useful structural modification, which in combination with other modifications may ultimately render the dihydroazulene/vinylheptafulvene system suitable for real MOST systems.

Conflicts of interest

There are no conflicts to declare.

Acknowledgements

University of Copenhagen is acknowledged for financial support. Dr Marco Santella is thanked for assistance regarding fluorescence measurements.

Notes and references

1 (*a*) H.-D. Scharf, J. Fleischhauer, H. Leismann, I. Ressler, W. Schleker and R. Weitz, *Angew. Chem., Int. Ed. Engl.*, 1979, **18**, 652; (*b*) T. J. Kucharski, Y. Tian, S. Akbulatov and R. Boulatov, *Energy Environ. Sci.*, 2011, **4**, 4449; (*c*) K. Moth-Poulsen, in *Organic Synthesis and Molecular Engineering*, ed. M. B. Nielsen, Wiley, Hoboken, USA, 2014, pp. 179–196; (*d*) A. Lennartson, A. Roffey and K. Moth-Poulsen, *Tetrahedron Lett.*, 2015, **56**, 1457.

2 Z.-I. Yoshida, *J. Photochem.*, 1985, **29**, 27.

3 (*a*) J. Daub, T. Knöchel and A. Mannschreck, *Angew. Chem., Int. Ed. Engl.*, 1984, **23**, 960; (*b*) T. Mrozek, A. Ajayaghosh and J. Daub, Optoelectronic Molecular Switches Based on Dihydroazulene–Vinylheptafulvene (DHA–VHF), in *Molecular Switches*, ed. B. L. Feringa, Wiley-VCH, Weinheim, 2001, pp. 63–106; (*c*) S. L. Broman and M. B. Nielsen, *Phys. Chem. Chem. Phys.*, 2014, **16**, 21172.

4 (*a*) H. Görner, C. Fischer, S. Gierisch and J. Daub, *J. Phys. Chem.*, 1993, **97**, 4110; (*b*) H. Görner, C. Fischer and J. Daub, *J. Photochem. Photobiol., A*, 1995, **85**, 217.

5 O. Schalk, S. L. Broman, M. Å. Petersen, D. V. Khakhulin, R. Y. Brogaard, M. B. Nielsen, A. E. Boguslavskiy, A. Stolow and T. I. Sølling, *J. Phys. Chem. A*, 2013, **117**, 3340.

6 S. L. Broman, S. L. Brand, C. R. Parker, M. Å. Petersen, C. G. Tortzen, A. Kadziola, K. Kilså and M. B. Nielsen, *ARKIVOC*, 2011, **ix**, 51.

7 S. L. Broman, M. Jevric and M. B. Nielsen, *Chem.–Eur. J.*, 2013, **19**, 9542.

8 (*a*) S. L. Broman, O. Kushnir, M. Rosenberg, A. Kadziola, J. Daub and M. B. Nielsen, *Eur. J. Org. Chem.*, 2015, 4119; (*b*) M. Cacciarini, A. B. Skov, M. Jevric, A. S. Hansen, J. Elm, H. G. Kjaergaard, K. V. Mikkelsen and M. B. Nielsen, *Chem.–Eur. J.*, 2015, **21**, 7454.

9 S. T. Olsen, J. Elm, F. E. Storm, A. N. Gejl, A. S. Hansen, M. H. Hansen, J. R. Nikolajsen, M. B. Nielsen, H. G. Kjaergaard and K. V. Mikkelsen, *J. Phys. Chem. A*, 2015, **119**, 896.

10 (*a*) M. H. Hansen, J. Elm, S. T. Olsen, A. N. Gejl, F. E. Storm, B. N. Frandsen, A. B. Skov, M. B. Nielsen, H. G. Kjaergaard and K. V. Mikkelsen, *J. Phys. Chem. A*, 2016, **120**, 9782; (*b*) A. S. Gertsen, S. T. Olsen, S. L. Broman, M. B. Nielsen and K. V. Mikkelsen, *J. Phys. Chem. C*, 2017, **121**, 195; (*c*) M. Koerstz, J. Elm and K. V. Mikkelsen, *J. Phys. Chem. A*, 2017, **121**, 3148.

11 J. Gurke, M. Quick, N. P. Ernsting and S. Hecht, *Chem. Commun.*, 2017, **53**, 2150.

12 For a recent review on the control of diarylethene photoswitches by external stimuli, see: S.-Z. Pu, Q. Sun, C.-B. Fan, R.-J. Wang and G. Liu, *J. Mater. Chem. C*, 2016, **4**, 3075.

13 (*a*) L. Gobbi, P. Seiler and F. Diederich, *Angew. Chem., Int. Ed.*, 1999, **38**, 674; (*b*) L. Gobbi, P. Seiler, F. Diederich, V. Gramlich, C. Boudon, J.-P. Gisselbrecht and M. Gross, *Helv. Chim. Acta*, 2001, **84**, 743; (*c*) M. Å. Petersen, S. L. Broman, K. Kilså, A. Kadziola and M. B. Nielsen, *Eur. J. Org. Chem.*, 2011, 1033.

14 The steps towards **11** follow known procedures: (*a*) J. Epsztajn and A. Bieniek, *J. Chem. Soc., Perkin Trans. 1*, 1985, 213; (*b*) D. R. Boyd, R. J. H. Davies, L. Hamilton and J. J. McCullough, *J. Chem. Soc.*, 1992, 31; (*c*) C.-Y. Cheng, L.-W. Hsin and J.-P. Liou, *Tetrahedron*, 1996, **52**, 10935.

15 M. J. Frisch, G. W. Trucks, H. B. Schlegel, G. E. Scuseria, M. A. Robb, J. R. Cheeseman, G. Scalmani, V. Barone, G. A. Petersson, H. Nakatsuji, X. Li, M. Caricato, A. V. Marenich, J. Bloino, B. G. Janesko, R. Gomperts, B. Mennucci, H. P. Hratchian, J. V. Ortiz, A. F. Izmaylov, J. L. Sonnenberg, D. Williams-Young, F. Ding, F. Lipparini, F. Egidi, J. Goings, B. Peng, A. Petrone, T. Henderson, D. Ranasinghe, V. G. Zakrzewski, J. Gao, N. Rega, G. Zheng, W. Liang, M. Hada, M. Ehara, K. Toyota, R. Fukuda, J. Hasegawa, M. Ishida, T. Nakajima, Y. Honda, O. Kitao, H. Nakai, T. Vreven, K. Throssell, J. A. Montgomery Jr, J. E. Peralta, F. Ogliaro, M. J. Bearpark, J. J. Heyd, E. N. Brothers, K. N. Kudin, V. N. Staroverov, T. A. Keith, R. Kobayashi, J. Normand, K. Raghavachari, A. P. Rendell, J. C. Burant, S. S. Iyengar, J. Tomasi, M. Cossi, J. M. Millam, M. Klene, C. Adamo, R. Cammi, J. W. Ochterski, R. L. Martin, K. Morokuma, O. Farkas, J. B. Foresman and D. J. Fox, *Gaussian 16, Revision A.03*, Gaussian, Inc., Wallingford CT, 2016.

16 M. J. Frisch, G. W. Trucks, H. B. Schlegel, G. E. Scuseria, M. A. Robb, J. R. Cheeseman, G. Scalmani, V. Barone, G. A. Petersson, H. Nakatsuji, X. Li, M. Caricato, A. Marenich, J. Bloino, B. G. Janesko, R. Gomperts, B. Mennucci, H. P. Hratchian, J. V. Ortiz, A. F. Izmaylov, J. L. Sonnenberg, D. Williams-Young, F. Ding, F. Lipparini, F. Egidi, J. Goings, B. Peng, A. Petrone, T. Henderson, D. Ranasinghe, V. G. Zakrzewski, J. Gao, N. Rega, G. Zheng, W. Liang, M. Hada, M. Ehara, K. Toyota, R. Fukuda, J. Hasegawa, M. Ishida, T. Nakajima, Y. Honda, O. Kitao, H. Nakai, T. Vreven, K. Throssell, J. A. Montgomery Jr, J. E. Peralta, F. Ogliaro, M. Bearpark,

J. J. Heyd, E. Brothers, K. N. Kudin, V. N. Staroverov, T. Keith, R. Kobayashi, J. Normand, K. Raghavachari, A. Rendell, J. C. Burant, S. S. Iyengar, J. Tomasi, M. Cossi, J. M. Millam, M. Klene, C. Adamo, R. Cammi, J. W. Ochterski, R. L. Martin, K. Morokuma, O. Farkas, J. B. Foresman and D. J. Fox, *Gaussian 09, Revision E.01*, Gaussian, Inc., Wallingford CT, 2016.

17 K. Raghavachari, J. S. Binkley, R. Seeger and J. A. Pople, *J. Chem. Phys.*, 1980, **72**, 650.